Bioactivity and molecular targets of novel substituted quinolines in murine and human tumor cell lines *in vitro*

ELISABETH M. PERCHELLET[1], KYLE R. CROW[1], GUNJAN GAKHAR[2], THU ANNELISE NGUYEN[2], AIBIN SHI[3], DUY H. HUA[3] and JEAN-PIERRE H. PERCHELLET[1]

[1]Anti-Cancer Drug Laboratory, Division of Biology, Ackert Hall, Departments of [2]Diagnostic Medicine and Pathobiology, and [3]Chemistry, Kansas State University, Manhattan, KS 66506-4901, USA

Received October 9, 2009; Accepted November 17, 2009

DOI: 10.3892/ijo_00000543

Abstract. Substituted quinolines (PQ code number), which reduce colony formation and increase gap junctional intercellular communication, were tested for their ability to interact with various molecular targets in murine and human tumor cell lines *in vitro*. Various markers of tumor cell metabolism, DNA fragmentation, mitotic disruption, apoptosis induction and growth factor receptor signaling pathways were assayed *in vitro* to evaluate drug cytotoxicity. Based on its ability to inhibit the metabolic activity of suspension cultures of leukemic L1210 cells at days 2 and 4 *in vitro*, **PQ1** succinic acid salt is the most effective antiproliferative agent among the synthetic quinoline analogs tested. Moreover, antiproliferative **PQ1** is effective across a spectrum of monolayer cultures of pancreatic Pan02, epidermoid A-431 and mammary SK-BR-3 and BT-474 tumor cells. **PQ1** also blocks Ki-67 expression, a marker of tumor cell proliferation. A 1.5- to 3-h treatment with **PQ1** is sufficient to inhibit the incorporations of [^{3}H]-thymidine into DNA, [^{3}H]-uridine into RNA and [^{3}H]-leucine into protein used to assess the rates of macromolecule syntheses over a 0.5- or 1-h period of pulse-labeling in L1210 tumor cells. A 15-min pretreatment with **PQ1** inhibits the cellular transport of both purine and pyrimidine nucleosides over a 30-sec period *in vitro*, suggesting that **PQ1** may prevent the incorporation of [^{3}H]-adenosine and [^{3}H]-thymidine into DNA because it rapidly blocks the uptake of these nucleosides by the tumor cells. Since **PQ1** does not reduce the fluorescence of the ethidium bromide-DNA complex, it does not directly bind to or destabilize double-stranded DNA. Over a 6- to -48-h period, **PQ1** has very little effect on the mitotic index of L1210 cells but stimulates the formation of many binucleated cells and a few micronuclei, suggesting that this compound might increase mitotic abnormality, induce chromosomal damage or missegregation, and block cytokinesis. The fact that **PQ1** induces initiator caspase-2 and effector caspase-3 activities and poly(ADP-ribose) polymerase-1 cleavage within 1-4 h and internucleosomal DNA fragmentation within 24 h in L1210 cells suggests that this antitumor drug can trigger the early and late events required for cells to undergo apotosis. Whole-cell immunodetection and Western blot analysis indicate that, in contrast to 17-(allylamino)-17-demethoxygeldanamycin and radicicol, **PQ1** fails to down-regulate the protein level at 24 h and autophosphorylation at 3 h of membrane-anchored HER1 in A-431 cells and HER2 in SK-BR-3 cells, suggesting that this antitumor compound is unlikely to interact with and inhibit Hsp90 and the epidermal growth factor (EGF) receptor signaling pathways. In conclusion, antiproliferative **PQ1** is effective against a spectrum of tumor cells and might interact with various membrane and nuclear targets to enhance gap junctions, inhibit nucleoside transport and block cytokinesis but does not appear to disrupt the EGF receptor-mediated signaling pathways to induce growth arrest and apoptosis.

Correspondence to: Dr J.-P. Perchellet, Anti-Cancer Drug Laboratory, Division of Biology, Ackert Hall, Kansas State University, Manhattan, KS 66506-4901, USA
E-mail: jpperch@ksu.edu

Key words: synthetic quinolines, tumor cell proliferation, Ki-67 expression, macromolecule syntheses, nucleoside transport, DNA interaction and fragmentation, mitotic and binucleated cells, caspases, poly(ADP-ribose) polymerase-1, apoptosis, human epidermal growth factor receptors

Introduction

A new class of substituted quinolines (code name PQ) has recently been reported to induce interesting anticancer activities involving the enhancement of gap junctional intercellular communication (GJIC) in breast cancer cells (1,2). GJIC, which is responsible for the direct traffic of ions and molecules with molecular weights <1,200 Da, is achieved through two hemichannels on the surface of opposing cells (3,4). Using Autodock computational docking software, a number of synthetic PQs were observed to bind to the inert core of the hexameric hemichannel of the gap junction, which is formed by the association of a family of six proteins, the connexins. As GJIC is downregulated by oncogenes and upregulated by tumor suppressor genes, and inhibition of GJIC contributes to carcinogenesis, restoration of GJIC may represent a desirable target for anticancer drugs (5-9). Since tumor cells have reduced or altered GJIC capacity (10), synthetic PQs were tested for their ability to enhance GJIC and inhibit tumor cell

growth. PQ compounds, which have a relatively high binding affinity for connexin 43 (Cx43) and may decrease its phosphorylation, were demonstrated by scrape load/dye transfer assay to increase GJIC in T-47D mammary tumor cells but not in normal mammary epithelial cells (2). Moreover these PQs significantly reduced the ability of T-47D human breast cancer cells to grow and form colonies on soft agar *in vitro* and to develop as xenograft tumors in nude mice *in vivo* (2). Because antitumor compounds that enhance GJIC activity are rare, the present study was undertaken to further characterize the bioactivity and molecular targets of synthetic PQs in a spectrum of murine and human tumor cell lines *in vitro*. For instance, it was of interest to determine whether antitumor PQs that interact with cell surface gap junctions and inhibit tumor cell growth would act as small molecule inhibitors of other membrane-anchored proteins, such as representative members of the family of human epidermal growth factor (EGF) receptors (HERs) that mediate critical intracellular signaling pathways of tumor cell proliferation and angiogenesis. Hence, in an attempt to identify the most potent antitumor lead compound of the series, several PQ structures were synthesized and compared with known anticancer drugs for their ability to inhibit the proliferation of various tumor cells, including those that overexpress ligand-dependent HER1 and ligand-independent HER2 and are sensitive to the 90-kDa heat shock protein (Hsp90) and HER inhibitors 17-(allylamino)-17-demethoxygeldanamycin (17-AAG) and radicicol. Since the fraction of Ki-67-positive tumor cells is often correlated with the clinical course of cancer, it was also of interest to determine whether PQ treatment would inhibit the expression of human Ki-67 nuclear protein, which is an excellent marker of tumor cell proliferation (11).

Materials and methods

Drug treatment, cell culture and proliferation assay. As reported previously, PQ analogues were synthesized by a modification of the procedure starting from 4-acetaminoanisole (1,2,12,13). Solutions of synthetic PQs and known anticancer drugs, daunorubicin (DAU), mitoxantrone (Mitox), vincristine (VCR), taxol, 17-AAG and radicicol (all from Sigma-Aldrich, St. Louis, MO, USA), were dissolved and serially diluted in dimethyl sulfoxide. Suspension cultures of murine L1210 lymphocytic leukemia cells (ATCC, Manassas, VA, USA) and monolayer cultures of murine Pan02 pancreatic ductal adenocarcinoma (DCTD Tumor Repository, NCI, USA) and human T-47D mammary ductal carcinoma, HER1-overexpressing A-431 epidermoid carcinoma, and HER2-overexpressing SK-BR-3 breast adenocarcinoma and BT-474 breast ductal carcinoma cells (all from ATCC) were incubated at 37˚C in a humidified atmosphere containing 5% CO_2 and maintained in continuous exponential growth by twice-a-week passage in RPMI-1640 medium supplemented with 10% fetal bovine calf serum (FCS; Atlanta Biologicals, Norcross, GA, USA) and penicillin (100 IU/ml)-streptomycin (100 μg/ml). L1210 leukemia cell suspensions were grown in triplicate in 48-well Costar cell culture plates for 2 and 4 days in the presence or absence (control) of serial concentrations of drugs to evaluate their antiproliferative activity. Adherent Pan02, A-431, SK-BR-3 and BT-474 tumor cells were collected by trypsinization, resuspended in fresh FCS-containing RPM-1640 medium, plated in 48-well Costar cell culture plates, and allowed to attach for 24 h before being incubated for an additional 2-4 days in the presence or absence (control) of the above drugs. Since compounds were supplemented to the culture medium in 1-μl aliquots, the concentrations of vehicle in the final incubation volume (0.5 ml) never exceeded 0.2% and did not interfere with the data. Decreasing concentrations of cells, such as 55,000 and 4,688 L1210 cells/0.5 ml, 7,500 and 1,875 Pan02 cells/0.5 ml, 7,500 and 1,875 A-431 cells/0.5 ml, 15,000 and 5,000 SK-BR-3 cells/0.5 ml or 15,625 and 7,812 BT-474 cells/0.5 ml/well, were initially plated in triplicate at time 0 in order to collect control samples with approximatively equal cell densities after 2 and 4 days in culture, respectively. The proliferation of drug-treated tumor cells was assessed from their mitochondrial ability to bioreduce the 3-(4,5-dimethylthiazol-2-yl)-5-(3-carboxymethoxyphenyl)-2-(4-sulfophenyl)-2*H*-tetrazolium (MTS) reagent (Promega, Madison, WI, USA) in the presence of phenazine methosulfate (PMS; Sigma) into a water-soluble formazan product that absorbs at 490 nm (14). After 2 or 4 days in culture, control and drug-treated L1210, Pan02, A-431, SK-BR-3 or BT-474 cell samples were further incubated at 37˚C for 1.5-3.0 h in the dark in the presence of 0.1 ml of MTS:PMS (2:0.1) reagent and their relative metabolic activity was estimated by recording the absorbance at 490 nm, using a Cambridge model 750 automatic microplate reader (Packard, Downers Grove, IL, USA). Blank values for culture medium supplemented with MTS:PMS reagent in the absence of cells were subtracted from the results. Data of all biochemical experiments were analyzed using Student's t-test with the level of significance set at $P<0.05$.

Immunofluorescence and confocal microscopy. For Ki-67 expression, T-47D cells were grown on coverslips in 6-well plates in RPMI media and incubated at 37˚C for 24, 48 and 72 h in the presence or absence (control) of PQ compound. After fixation with 2% paraformaldehyde for 20 min followed by neutralization with 50 mM glycine for 5 min, the cells were lysed with 0.1% Triton X-100 for an additional 10 min. The cells were washed with Ca^{2+}/Mg^{2+}-free Dulbecco's phosphate-buffered saline (PBS), blocked with 2.5% bovine serum albumin (BSA) in PBS for 2 h and then incubated with rabbit anti-Ki-67 (H300) primary polyclonal antibody (pAb) (1:250; Santa Cruz Biotechnology, Santa Cruz, CA, USA) for 15 h at 4˚C. After incubation for a minute with 4',6'-diamidino-2-phenylindole (DAPI), a blue-fluorescent DNA stain, the cells were then incubated with Alexa fluor 488 dye-labeled anti-rabbit secondary antibody (Ab) conjugate (Molecular Probes, Eugene, OR, USA) for 4 h at 4˚C. Samples were sealed and analyzed by fluorescence microscopy for nuclear morphology (DAPI staining) and Ki-67 expression (immunolabeling), using a Zeiss LSM 510 META confocal microscope (Carl Zeiss, Thornwood, NY, USA) equipped with micromanipulator (Narishige International, East Meadow, NY, USA).

Macromolecule syntheses and nucleoside transport. To estimate the rate of DNA synthesis, L1210 cells were resus-

pended in fresh FCS-containing RPM-1640 medium at a density of $0.5x10^5$ cells/0.5 ml, incubated at 37˚C for 90 min in the presence or absence (control) of drugs and then pulse-labeled for an additional 30 min with 1 μCi of [methyl-^{3}H]-thymidine (52 Ci/mmol; GE Healthcare-Amersham, Piscataway, NJ, USA) (15). For RNA and protein syntheses, cells were incubated at 37˚C for 3 h in the presence or absence of drugs and then pulse-labeled for an additional 1 h with 2 μCi of [5,6-^{3}H]-uridine (35 Ci/mmol; Perkin-Elmer, Boston, MA, USA) or 2.5 μCi of L-[3,4,5-^{3}H]-leucine (115 Ci/mmol; Perkin-Elmer), respectively (15). The incubations were terminated by the addition of 0.5 ml of 10% trichloroacetic acid (TCA). After holding on ice for 15 min, the acid-insoluble material was recovered over Whatman GF/A glass microfiber filters and washed thrice with 2 ml of 5% TCA and twice with 2 ml of 100% EtOH. After drying the filters, the radioactivity bound to the acid-precipitable material was determined by liquid scintillation counting (LSC) in 6 ml of Bio-Safe NA (Research Products International, Mount Prospect, IL, USA) (15). For nucleoside transport, L1210 cells ($1.2x10^6$ cells/ml) were preincubated for 15 min at 37˚C in the presence or absence (control) of drugs and then exposed to 1 μCi of [2,8-^{3}H]-adenosine (25 Ci/mmol; Moravek Biochemicals, Brea, CA, USA) or [methyl-^{3}H]-thymidine for only 30 sec to, respectively, assess the cellular uptake of purine and pyrimidine nucleosides over such very short period of time (15,16). Reactions were diluted with 2 ml of ice-cold PBS and the unincorporated radiolabel was removed by centrifugation at 200 g for 10 min. After washing thrice with 2 ml of ice-cold PBS, intact cell pellets were harvested by centrifugation and incubated for 30 min in 1 ml of hypotonic lysis buffer (HLB) containing 10 mM Tris-HCl, pH 8.0, 1 mM EDTA and 0.2% Triton X-100. Cell lysates were mixed with 6 ml of Bio-Safe II (Research Products International) to estimate the cellular uptake of [^{3}H]-adenosine or [^{3}H]-thymidine by LSC. Drug inhibition was expressed as % of [^{3}H]-adenosine or [^{3}H]-thymidine transported into vehicle-treated control tumor cells over a similar 30-sec period (15,16).

DNA binding and fragmentation assays. An ethidium bromide (EB) displacement assay was used to assess the eventual DNA-binding potencies of PQ compounds, based on the IC_{50} concentrations of drugs that cause a 50% reduction in the fluorescence of the DNA-EB complex at 525 nm excitation/600 nm emission (17). The fluorescence of EB, which is extremely low when unbound in water, is boosted 25-fold after binding and intercalating in the hydrophobic environment of the intact double-stranded DNA. Since a highly fluorescent complex is formed within milliseconds between DNA and EB, any drug directly binding to and/or damaging DNA would disrupt EB intercalation and compromise the fluorescence of this EB-DNA complex. The reaction mixtures (200 μl), containing final concentrations of 20 μg/ml calf thymus (ct) DNA (Sigma) and 1 μg/ml EB (Sigma) in 5 mM Tris-HCl buffer, pH 7.6, with 0.5 mM EDTA, were pipeted into 96-well Costar white opaque polystyrene assay plates and, after incubation in the presence or absence (control) of drugs for 30 min at room temperature, the fluorescence of the EB-DNA complex was detected at 525 nm excitation and 600 nm emission, using a Cary Eclipse fluorescence spectrophotometer equipped with microplate reader accessory (Varian, Walnut Creek, CA, USA).

Drug-induced DNA cleavage was determined by intact chromatin precipitation, using L1210 cells which were pre-labeled with 1 μCi of [^{3}H]-thymidine for 2 h at 37˚C, washed with 3x1 ml of ice-cold PBS, collected by centrifugation, resuspended in fresh medium at a density of $1.2x10^6$ cells/ml, and then incubated at 37˚C for 24 h in the presence or absence of drugs (16,18). After centrifugation at 200 g for 10 min to discard the drugs and wash the cells, the cell pellets were lysed for 20 min in 0.5 ml of ice-cold HLB, and centrifuged at 12,000 g for 15 min to collect the supernatants. The radioactivity in the supernatants (detergent-soluble low molecular weight DNA fragments) and the pellets (intact chromatin DNA) was determined by LSC. Before being counted in 6 ml of Bio-Safe NA, the intact pelleted chromatin was incubated for 2 h at 60˚C in the presence of 0.6 ml of NCS tissue solubilizer (Amersham) (16,18). For internucleosomal DNA fragmentation, L1210 cells were incubated at 37˚C for 24 h in the presence or absence of drugs and DNA was extracted from samples with equal cell densities ($2x10^6$ cells/ml), using a salting out procedure (16,18). Cell pellets were washed twice with PBS, lysed overnight at 37˚C in 0.34 ml of 10 mM Tris-HCl, pH 8.0, containing 2 mM EDTA, 400 mM NaCl, 1% SDS, and proteinase K (0.5 mg/ml), vortexed for 15 sec with 0.1 ml of 6 M NaCl and centrifuged (2,500 g x 30 min), and the DNA was precipitated from the supernatants (0.44 ml) with 0.88 ml of 100% EtOH for 15 min at 4˚C. After centrifugation (14,000 g x 15 min) at 4˚C, the air-dried DNA pellets were dissolved in 0.34 ml of 10 mM Tris-HCl, pH 8.0, with 1 mM EDTA (TE buffer) and incubated for 2 h at 37˚C in the presence of RNase (0.1 mg/ml). After another round of EtOH precipitation and centrifugation, the final air-dried pellets were dissolved in 50 μl of TE buffer and their DNA concentrations determined spectrophotometrically at 260 nm. Equal amounts of DNA samples (6 μg/7.5 μl TE buffer) were mixed with 1.5 μl of 10 mM Tris-HCl, pH 7.5, containing 50 mM EDTA, 10% Ficoll 400, and 0.4% Orange G, and loaded on each lane. About 0.5 μg of 100 bp DNA ladder and 0.75 μg of λ DNA/*Eco*RI + *Hin*dIII (both from Promega) were similarly applied to each gel to provide size markers in the range 100-1,500 and 125-21,226 bp, respectively. Horizontal electrophoresis of DNA samples was performed for 3.7 h at 60 V in 1.5% agarose gels containing EB (1 μg/ml) with 90 mM Tris-HCl, pH 8.0, containing 90 mM boric acid and 2 mM EDTA as a running buffer. The DNA fragments were visualized and photographed with Polaroid 667 film under UV light at 312 nm, using a FisherBiotech model 88A variable-intensity UV transilluminator (16,18).

Mitotic index and abnormalities. To determine the mitotic index, L1210 cells ($0.5x10^6$/0.5 ml of FCS-containing RPM-1640 medium) were incubated in triplicate for various periods of time at 37˚C in the presence or absence (control) of serial concentrations of experimental drugs or known microtubule-disrupting agents, collected by centrifugation (200 g x 10 min), and resuspended in 1 ml of hypotonic 75 mM KCl for 20 min at 4˚C. After fixation in 1 ml of MeOH:acetic acid (3:1), the final cell pellets were collected by centrifugation, resuspended in 75 μl of MeOH:acetic acid (3:1), dispensed

onto glass slides, air dried, and stained by spreading 40 μl of 0.1% crystal violet under a coverslip (15). Mitotic figures with condensed chromosomes were identified microscopically and published criteria were followed to score binucleated cells and micronuclei (19). Cytokinesis-blocked binucleated cells contained either 2 separate nuclei of equal size, 2 nuclei that touched or overlapped with distinct nuclear boundaries, or 2 nuclei that were linked by a small nucleoplasmic bridge (19). Dot-like chromatin-containing structures in the cytoplasm, at least 1/3 smaller than the main nucleus, surrounded by a membrane either separated from or marginally overlapping the main nucleus, and having the same staining as the main nucleus were scored as micronuclei containing either a whole chromosome or an acentric chromosomal fragment (19). The frequencies of binucleated cells and micronuclei were used to estimate the ability of cytotoxic or genotoxic (mutagenic or clastogenic) drugs to block cytokinesis and induce chromosomal damage or missegregation (19). The % of cells in mitosis or binucleated cells were determined microscopically by counting a total of at least 2,000 cells/slide and the mitotic index or binucleated cell index were calculated as % of mitotic figures or binucleated cells in drug-treated cultures/% of mitotic figures or binucleated cells in vehicle-treated controls (15,19).

Fluorogenic assay of caspase activities. Control and drug-treated L1210 cells (10^6/ml) were incubated for 1-24 h at 37˚C, collected by centrifugation (200 g x 10 min), and washed with 1 ml of ice-cold PBS. The cell pellets were resuspended in chilled 10 mM HEPES buffer, pH 7.4, containing 100 mM NaCl, 100 mM KCl, 5 mM $MgCl_2$, 1 mM EDTA, 10 mM EGTA, 10% sucrose, 1 mM phenylmethylsulfonyl fluoride (PMSF), 1 mM dithiothreitol (DTT), and 100 μM digitonin (175 μl for caspase-3 assay and 120 μl for caspase-2 assay), and were lysed for 10 min on ice. The cell lysates were centrifuged (14,000 g x 20 min) at 4˚C to precipitate cellular debris and the supernatants were stored at -70˚C overnight (16,18). The caspase-2- and -3-like activities of the lysates were determined in reaction mixtures that contained 50 μl of lysis buffer (blank) or supernatant (control or drug-treated samples) and 50 μl of reaction buffer (100 mM HEPES, pH 7.5, containing 1 mM EDTA, 10 mM EGTA, 10% sucrose, and 10 mM DTT) and that were initiated by the addition of 5-μl aliquots of the respective 5 mM benzyloxycarbonyl (z)-Val-Asp-Val-Ala-Asp (VDVAD)-7-amino-4-trifluoromethylcoumarin (AFC) or 1 mM z-Asp-Glu-Val-Asp (DEVD)-AFC stocks of AFC-substrate conjugates (all from Calbiochem, La Jolla, CA, USA) (16,18). After incubation for 1 h at 37˚C in 96-well Costar white opaque polystyrene assay plates, the fluorescence of the free AFC released upon proteolytic cleavage of the substrate by the appropriate caspase was detected at 400-nm excitation and 505-nm emission, using a Cary Eclipse fluorescence spectrophotometer with microplate reader. Arbitrary fluorescence units were quantified with reference to calibration curves ranging from 0.01 to 6 nmol of AFC (from Sigma), the protein concentrations of the supernatants were determined using the BCA Protein Assay Kit (Pierce, Rockford, IL, USA), and the VDVAD- and DEVD-specific cleavage activities of the samples were expressed as nmol of AFC released/mg of protein (16,18).

Western blot analysis of poly(ADP-ribose) polymerase-1 (PARP-1) cleavage. Suspensions of control and drug-treated L1210 cells ($1.2x10^6$ cells/ml) were incubated for 1-20 h at 37˚C in 15x60 mm Falcon Petri dishes containing final volumes of 5 ml. For PARP-1 cleavage, $12x10^6$ tumor cells were collected by centrifugation, washed with 1 ml of PBS, lysed with 45 μl of 50 mM Tris-HCl buffer, pH 6.8, containing 250 mM NaCl, 1 mM $CaCl_2$, 50 mM NaF, 0.1% Triton X-100, 6 M urea, and protease inhibitors (10 μg leupeptin/ml, 8 μg aprotinin/ml, 1 mM PMSF and the complete EDTA-free protease inhibitor cocktail from Roche Diagnostics Corp., Indianapolis, IN, USA), and disrupted by sonication with a tapered microtip for 12 strokes at power level 4 (80% duty cycle), using a 250 W Vibra Cell Ultrasonic Processor (Sonics & Materials, Danbury, CT, USA) (16,18,20). The cell lysates were centrifuged (14,000 g x 15 min) and the protein concentrations of the cytosolic supernatants were determined with the BCA Protein Assay Kit. For PARP-1 cleavage, aliquots of supernatants containing equal 70-μg quantities of proteins were incubated with SDS sample loading buffer (final concentration 10% glycerol, 2% SDS, 5% ß-mercaptoethanol, 0.02% bromophenol blue) for 15 min at 65˚C, resolved by electrophoresis for 1 h at 175 V in a 8% SDS-polyacrylamide gel, and transferred for 90 min to a PVDF sequencing membrane (Immobilon-P^{SQ}; Millipore, Bedford, MA, USA) using a Panther model HEP1 Semidry Electroblotter (Owl Separation Systems, Portsmouth, NH, USA) (16,18,20). The blots were blocked with 5% non-fat dry milk in 20 mM Tris-HCl buffer, pH 7.4, with 0.9% NaCl (TBS), containing 0.05% of Tween-20 (TBST) for 90 min at room temperature. Immunodetections of PARP-1 or ß-actin were conducted at 4˚C overnight in TBST containing 2% of non-fat dry milk, using, respectively, 0.5 μg/ml of mouse anti-PARP-1 (Ab-2) primary monoclonal Ab (mAb) (C-2-10; Calbiochem), which recognizes both the full-length 115-116-kDa native PARP-1 protein and its 85- to 90-kDa cleavage fragment (16,18,20), or anti-ß-actin (AC-15) primary mAb (1:15,000 dilution; Sigma), which recognizes an epitope located on the N-terminal end of the ß-isoform of actin in a wide variety of tissues and species. After the blots had been rinsed thrice with TBST, incubated for 1 h at room temperature in TBST containing 2% of non-fat dry milk and goat anti-mouse secondary mAb conjugated with horseradish peroxidase (1:30,000 dilution; Oncogene, Boston, MA, USA), and rinsed again thrice with TBST, Kodak BioMax light film was used to develop images of the immunoreactive bands revealed by enhanced chemiluminescence (CL) staining, using the SuperSignal West Pico CL Substrate (Pierce). The integrated density values of the Western blots were compared by digital image analysis (Chemi Imager 5500 with AlphaEase FCTM software), using a MultiImage Light Cabinet (Alpha Inotech, San Leandro, CA, USA) (16,18,20). Detection of the 42-kDa band of ß-actin was performed as an internal control to confirm equal protein loading.

Immunodetection of HER1 and HER2 protein level and autophosphorylation. For whole cell immunodetection, A-431 or SK-BR-3 cells ($2x10^4$ cells/0.2 ml) were seeded into 96-well Nunc F96 MicroWell polystyrene white plates (Thermo Fisher Scientific, Waltham, MA, USA), allowed to attach

for 24 h at 37˚C, and then incubated for an additional period of 24 h in the presence or absence (control) of drugs. After removing the culture medium by suction, the adherent cells in each well were washed twice with 70 µl of TBST and incubated at 4˚C for 10 min in 50 µl of ice-cold MeOH. The MeOH was removed by washing with TBST (2x100 µl) and the plates were further incubated with 100 µl of SuperBlock (Pierce) for 1 h at room temperature. After aspirating the SuperBlock, the plates were then incubated overnight at 4˚C with primary Ab, either rabbit anti-HER1 pAb [EGFR (1005): sc-03] raised against a peptide mapping at the C-terminus of EGFR of human origin or mouse anti-HER2 mAb [Neu (9G6): sc-08] raised against a peptide mapping to an extracellular domain of Neu gp185 of human origin (both from Santa Cruz Biotechnology), at a 1:200 dilution in SuperBlock (100 µl/well). Each well was washed with TBST (2x100 µl) and incubated for 1 h at room temperature with both horseradish peroxidase-linked secondary mAb (1:1,000 dilution; Oncogene) and Hoechst 33342 reagent (1:5,000 dilution; Invitrogen, Molecular Probes) in 50 µl of SuperBlock (21). After washing with TBST (2x100 µl) to remove the unbound antibody and adding the SuperSignal West Pico CL Substrate (20 µl/well), plates were read within 5 min by scanning each well for 0.1 sec in the CL mode (425 nm) of a Cary Eclipse fluorescence microplate reader (21). Readings from wells where the primary pAb or mAb was omitted were used to subtract the background. Finally, the plates were read in the fluorescence mode (340 nm excitation/460 nm emission) of a Cary Exclipse fluorescence microplate reader (21). The relative fluorescence intensities of the Hoechst reagent-DNA complexes were used to normalize the relative CL unit values of the primary pAb- or mAb-antigen immune complexes bound to the horseradish peroxidase-linked secondary Ab in order to compare HER1 or HER2 protein levels on an equal cell number basis (21). And the ratio of relative luminescence:fluorescence for drug-treated cells was expressed as % of that for vehicle-treated control cells.

For Western blot analysis of HER1 and HER2 autophosphorylation, A-431 or SK-BR-3 cells ($1x10^6$ cells/5 ml) were respectively seeded into 15x60 mm Falcon Petri dishes, allowed to attach for 24 h at 37˚C, and then incubated for an additional period of 3 h in the presence or absence (control) of drugs. For A-431 cells, EGF (100 ng/ml; R&D Systems, Minneapolis, MN, USA) was added during the last 15 min of incubation. After removing the culture medium and washing with PBS (2x2 ml), $2x10^6$ adherent cells were collected by scraping and rinsing in a total volume of 4 ml of PBS, pelleted by centrifugation (800 g x 10 min) at 4˚C, resuspended in 1 ml of ice-cold PBS for transfer to 1.5-ml Eppendorf, and recentrifuged (2,000 g x 6 min) at 4˚C. Cell samples were lysed for 30 min at 4˚C with 65 µl of 50 mM Tris-HCl buffer, pH 7.4, containing 150 mM NaCl, 2 mM EDTA, 1 mM DTT, 10 mM NaF, 1% NP-40, 0.1% SDS, 1 mM sodium orthovanadate, 5 mM sodium pyrophosphate and the cocktail of protease inhibitors indicated above, and then disrupted by sonication. The cell lysates were centrifuged (14,000 g x 15 min) and the protein concentrations of the cytosolic supernatants were determined with the BCA Protein Assay Kit. Aliquots of supernatants containing equal 70-µg quantities of proteins were incubated with SDS sample loading buffer for 5 min at 90˚C and resolved by electrophoresis for 1.3 h at 200 V in a 8% SDS-polyacrylamide gel before wet transfer to Protran nitrocellulose membrane (Schleicher & Schuell BioScience, Keene, NH, USA) overnight at 4˚C, using the Mini Trans-Blot Cell system (Bio-Rad, Hercules, CA, USA). The non-specific binding sites were blocked with 5% BSA in TBST. First, immunodetections of phosphorylated HER1 (pHER1) or phosphorylated HER2 (pHER2) were conducted at 4˚C overnight in TBST containing 2% of BSA, using, respectively, 0.5 µg/ml of goat anti-pHER1 primary pAb [p-EGFR (Tyr 1173): sc-12351] raised against a short amino acid sequence containing phosphorylated Tyr 1173 of EGFR of human origin or rabbit anti-pHER2 primary pAb [p-Neu (Tyr 1248-R): sc-12352-R] raised against a short amino acid sequence containing phosphorylated Tyr 1248 of Neu of human origin (both from Santa Cruz Biotechnology). The blots were then incubated with horseradish peroxidase-linked secondary mAb and the bands of immunoreactive proteins revealed by the enhance CL detection reagent as described above. In the same experiments, blots were also respectively probed overnight with rabbit anti-HER1 primary pAb or mouse anti-HER2 primary mAb, and the horseradish peroxidase-linked secondary mAb incubation and enhanced CL detection repeated, to confirm equal loading of receptor or assess and compare the levels of receptor autophosphorylation after correction with the levels of HER1 or HER2 protein loaded.

Results

Inhibition of tumor cell proliferation. The chemical structures and code names of the 11 substituted quinolines synthesized and tested for their ability to inhibit tumor cell proliferation *in vitro* are depicted in Fig. 1. General methods for organic synthesis of these compounds have been reported (1). All compounds tested at 4 or 25 µM, except **PQ2** and **PQ5** (data not shown), inhibited the mitochondrial ability of L1210 leukemic cells to metabolize the MTS:PMS reagent (Fig. 2). On an equal concentration basis, **PQ1** (4 µM inhibits by 75-99% at days 2-4), which is a more effective antiproliferative agent than PQ3 (25 µM inhibits by 84-99% at days 2-4) and is clearly the most potent lead antitumor compound of the series in the L1210 tumor system (Fig. 2), was selected for further studies. Indeed, antiproliferative **PQ1** retains its effectiveness in the low µM range across a spectrum of pancreatic, epidermoid and mammary tumor cell lines (Fig. 3). Inhibition of the metabolic activity of L1210 and SK-BR-3 tumor cells by **PQ1** is significant at 1.6 µM (data not shown), maximal or near maximal at 4 µM and more pronounced after 4 than 2 days in culture, suggesting that the antitumor activity of this drug is a combination of concentration and duration of action (Figs. 2 and 3). However, when tested as positive controls in the same experiments, established anticancer drugs like DAU, Mitox and radicicol inhibit the growth of various tumor cell lines at lower nM concentrations (Figs. 2 and 3). Interestingly, the antiproliferative activity of 17-AAG is comparable to that of **PQ1** in the low µM range in L1210 cells (Fig. 2) but improves dramatically in the nM range in SK-BR-3 (Fig. 3) and A-431 or BT-474 cells (data not shown) that may need HER1 or HER2 overexpression and stimulation for their growth. But this is not the case for

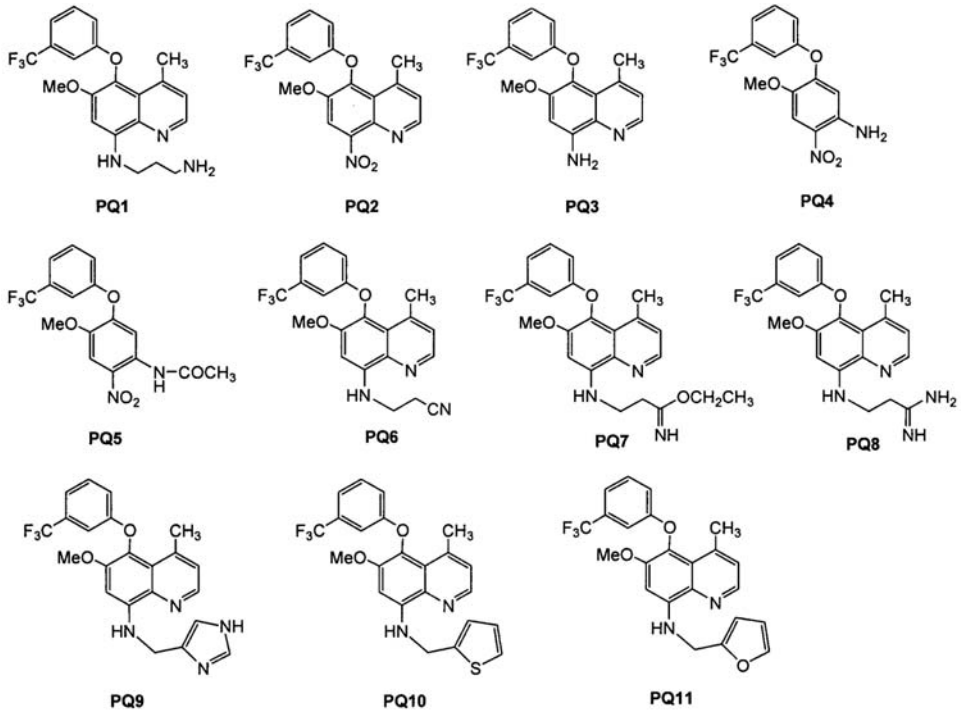

Figure 1. Chemical structures and code numbers of novel substituted quinolines.

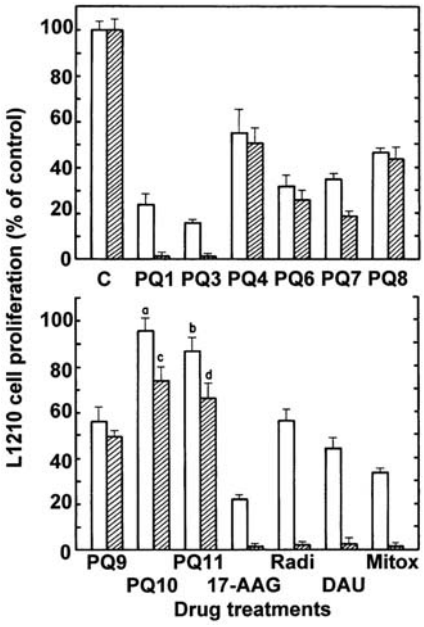

Figure 2. Comparison of the abilities of 4 μM **PQ1** and 25 μM concentrations of other substituted quinolines (PQ code number) to inhibit the metabolic activity of L1210 tumor cells at days 2 (open columns) and 4 (striped columns) *in vitro*. The inhibitions of L1210 cell proliferation caused by 6.6 nM Mitox, 41 nM DAU or radicicol, and 4 μM 17-AAG were used as positive controls. Cell proliferation results were expressed as % of the net absorbance of MTS/formazan after bioreduction by vehicle-treated control (C) cells after 2 ($A_{490\ nm}$ = 1.251±0.053, 100±4.2%) and 4 ($A_{490\ nm}$ = 1.125±0.052, 100±4.6%) days in culture. The blank values ($A_{490\ nm}$ = 0.426 at day 2 and 0.439 at day 4) for cell-free culture medium supplemented with MTS:PMS reagent were subtracted from the results. Bars, means ± SD (n=3). [a]Not different from control; [b]P<0.05, [c]P<0.01 and [d]P<0.005, smaller than respective controls.

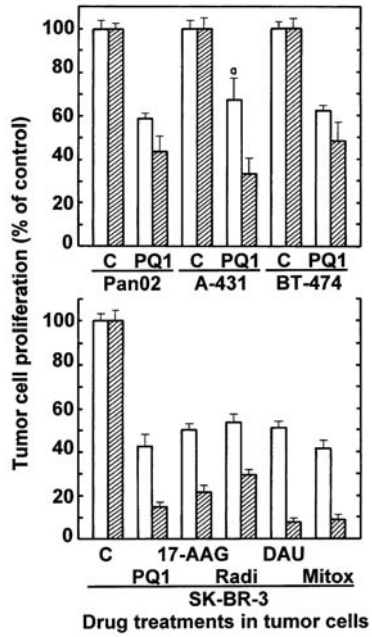

Figure 3. Comparison of the abilities of 4 μM **PQ1** to inhibit the metabolic activity of Pan02, A-431, BT-474 and SK-BR-3 tumor cells at days 2 (open columns) and 4 (striped columns) *in vitro*. The inhibitions of SK-BR-3 cell proliferation caused by 41 nM Mitox and 102 nM DAU, 17-AAG or radicicol were used as positive controls. Results were respectively expressed as % of control Pan02 cell proliferation ($A_{490\ nm}$ = 1.508±0.059, 100±3.9% at day 2 and $A_{490\ nm}$ = 1.186±0.037, 100±3.1% at day 4) after subtracting the blanks ($A_{490\ nm}$ = 0.380 at day 2 and 0.312 at day 4), % of control A-431 cell proliferation ($A_{490\ nm}$ = 1.377±0.054, 100±3.9% at day 2 and $A_{490\ nm}$ = 1.074±0.050, 100±4.7% at day 4) after subtracting the blanks ($A_{490\ nm}$ = 0.348 at day 2 and 0.338 at day 4), % of control BT-474 cell proliferation ($A_{490\ nm}$ = 1.074±0.033, 100±3.1% at day 2 and $A_{490\ nm}$ = 1.065±0.051, 100±4.8% at day 4) after subtracting the blanks ($A_{490\ nm}$ = 0.444 at day 2 and 0.451 at day 4), and % of control SK-BR-3 cell proliferation ($A_{490\ nm}$ = 1.269±0.043, 100±3.4% at day 2 and $A_{490\ nm}$ = 1.205±0.057, 100±4.7% at day 4) after subtracting the blanks ($A_{490\ nm}$ = 0.367 at day 2 and 0.393 at day 4). Bars, means ± SD (n=3). [a]P<0.01, smaller than control.

PQ1, for which no such shift in antiproliferative potency is detected between L1210 and the HER1- or HER2-over-expressing tumor cell lines, suggesting that, in contrast to

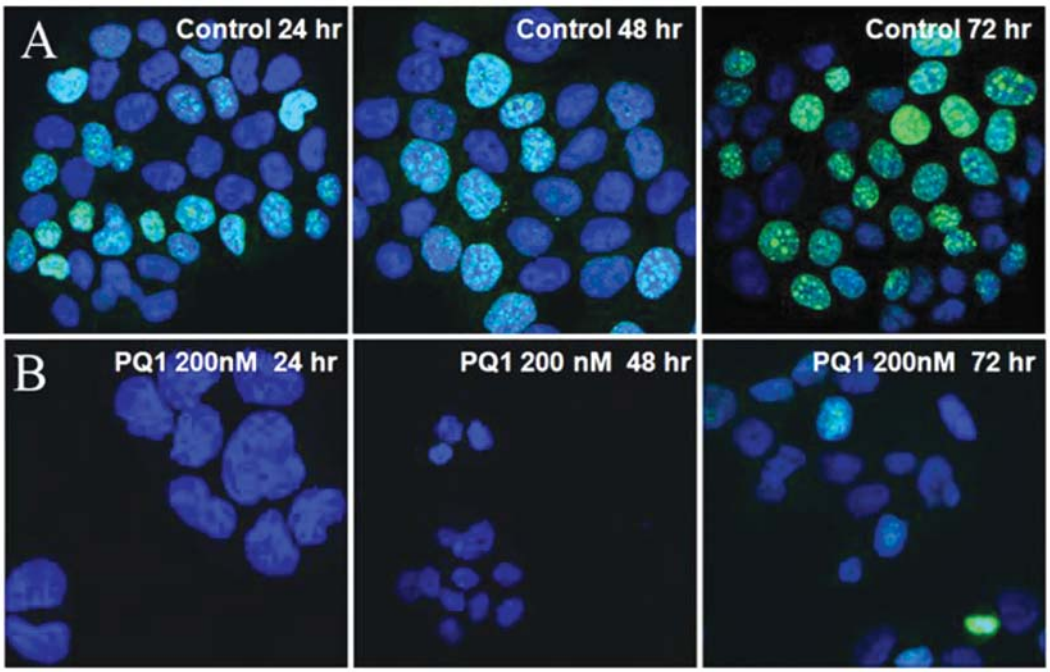

Figure 4. Confocal microscopy showing that **PQ1** inhibits the expression of the Ki-67 marker of tumor cell proliferation. T-47D cells were incubated for 24, 48 and 72 h in the absence (A, control) or presence of 200 nM **PQ1** (B) and analyzed for Ki-67 expression by immunolabeling and fluorescence microscopy. Blue fluorescence, nuclei labeled with DNA-binding DAPI dye. Green fluorescence, Ki-67 immune complex labeled with Alexa fluor 488 dye.

17-AAG, the antitumor activity of **PQ1** is not affected by the growth receptor dependency of the neoplastic cells (Figs. 2 and 3).

Inhibition of Ki-67 expression. Because the proliferation, viability and colony-forming ability of T-47D cells were previously shown to be inhibited by nM concentrations of **PQ1** (1,2), the ability of this compound to inhibit the Ki-67 marker of cell proliferation was determined in this mammary tumor cell line (Fig. 4). The Ki-67 nuclear protein, which is absent from resting cells (G_0), is present during all active phases of the cell cycle (G_1, S, G_2) and mitosis. Since Ki-67 expression is strictly associated with cell proliferation, it is an excellent marker for determining the growth fraction of tumor cell populations (11). As compared to the level of Ki-67 protein detected by immunolabeling and fluorescence microscopy in untreated T-47D control tumor cells, the remarkable inhibition of Ki-67 expression caused by 200 nM **PQ1** at 24-48 h and, to a lesser degree, at 72 h, suggests that this novel antiproliferative compound maintains surviving tumor cells in the resting stage and prevents them from re-entering the cell cycle (Fig. 4). After **PQ1** treatment, therefore, there are fewer tumor cells and they fail to express Ki-67 but the efficacy of **PQ1** at 200 nM may be shorter than 72 h (Fig. 4).

Inhibition of macromolecule syntheses and nucleoside transport. A 90-min treatment with **PQ1** is sufficient to inhibit the incorporation of [^{3}H]-thymidine into DNA used to assess the rate of DNA synthesis over a 30-min period of pulse-labeling in L1210 tumor cells *in vitro* (Fig. 5). Although it may be somewhat misleading to compare biological responses measured at very different times, the concentration-dependent inhibition of DNA synthesis by **PQ1**, which is maximal at

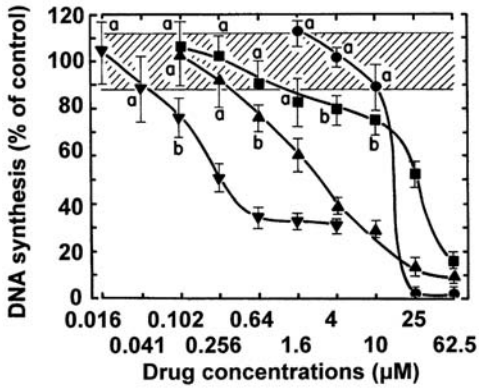

Figure 5. Comparison of the abilities of serial concentrations (plotted on a logarithmic scale) of **PQ1** (●), radicicol (■), 17-AAG (▲) and Mitox (▼) to inhibit the rate of incorporation of [^{3}H]-thymidine into DNA measured in L1210 cells over 30 min following a 90-min period of incubation at 37˚C *in vitro*. DNA synthesis in vehicle-treated control cells at 37˚C was 17,504±2,135 cpm (100±12.2%, striped area). The blank value (699±74 cpm) for control cells incubated and pulse-labeled at 2˚C with 1 μCi of [^{3}H]-thymidine has been subtracted from the results. Bars, means ± SD (n=3). [a]Not different from control; [b]P<0.05, smaller than control.

25 μM, suggests that the ability of this compound to prevent L1210 cells from synthesizing DNA at 2 h (Fig. 5) may play a role in its antiproliferative activity at days 2 and 4 (Fig. 2). Under similar experimental conditions, Mitox and 17-AAG are more effective inhibitors of DNA synthesis than **PQ1** but radicicol is not (Fig. 5). Interestingly, a 15-min treatment with 25-62.5 μM **PQ1** is sufficient to almost totally block the cellular uptake of [^{3}H]-adenosine (inhibition by 94-96%) and [^{3}H]-thymidine (inhibition by 75-99%) occurring over only 30 sec in L1210 cells *in vitro* (Fig. 6). In the same

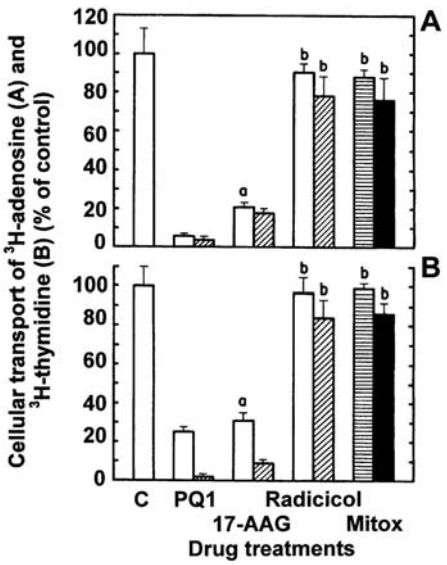

Figure 6. Comparison of the abilities of 15-min treatments with 25 (open columns) and 62.5 μM (diagonale stripes) concentrations of **PQ1**, 17-AAG and radicicol to inhibit the cellular uptake of purine (A) and pyrimidine (B) nucleosides into L1210 cells over 30 sec *in vitro*. Mitox was tested at 1.6 (horizontal stripes) and 4 μM (closed columns). The results were expressed as % of [^{3}H]-adenosine (56,090±7,180 cpm, 100±12.8% in A) or [^{3}H]-thymidine (19,338±1,856 cpm, 100±9.6% in B) transported into vehicle-treated control (C) cells over 30 sec. Bars, means ± SD (n=3). [a]P<0.0005, smaller than respective controls; [b]not different from respective controls.

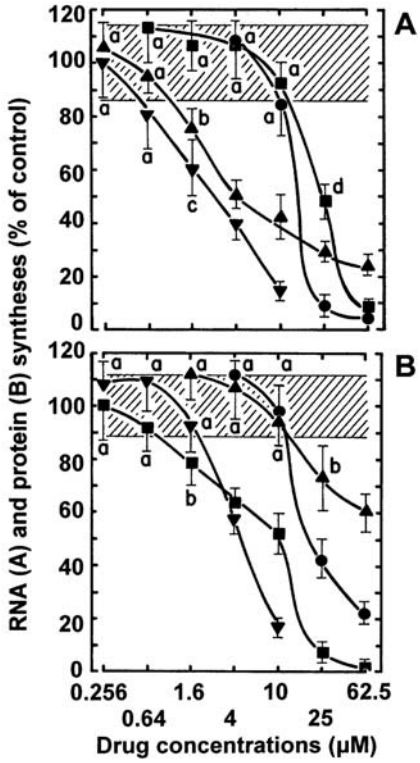

Figure 7. Comparison of the abilities of serial concentrations (logarithmic scale) of **PQ1** (●), radicicol (■), 17-AAG (▲) and Mitox (▼) to inhibit the rates of incorporation of [^{3}H]-uridine into RNA (A) and [^{3}H]-leucine into protein (B) measured in L1210 cells over 60 min following a 3-h period of incubation at 37°C *in vitro*. (A) RNA synthesis in vehicle-treated control cells at 37°C was 42,153±5,817 cpm (100±13.8%, striped area). The blank value (1,485±186 cpm) for control cells incubated and pulse-labeled at 2°C with 2 μCi of [^{3}H]-uridine has been subtracted from the results. Bars, means ± SD (n=3). [a]Not different from control; [b]P<0.05, [c]P<0.025 and [d]P<0.005, smaller than control. (B) Protein synthesis in vehicle-treated control cells at 37°C was 8,920±1,017 cpm (100±11.4%, striped area). The blank value (1,384±125 cpm) for control cells incubated and pulse-labeled at 2°C with 2.5 μCi of [^{3}H]-leucine has been subtracted from the results. [a]Not different from control; [b]P<0.05, smaller than control.

experiments, antitumor concentrations of radicicol and Mitox are ineffective but 17-AAG shares the ability of **PQ1** to block the cellular uptake of both purine (inhibition by 79-82%) and pyrimidine (inhibition by 69-91%) nucleosides (Fig. 6). These results suggest that antiproliferative **PQ1** and 17-AAG may decrease the incorporation of radiolabeled nucleosides into DNA at 2 h (Fig. 5) because they rapidly prevent the nucleoside transport system from incorporating these radiolabeled nucleosides into the L1210 cells within 15 min (Fig. 6). Besides DNA synthesis, a 3-h treatment with **PQ1** also inhibits, in a concentration-dependent manner, the rates of RNA and protein syntheses determined over 1-h periods of pulse-labeling in L1210 tumor cells *in vitro* (Fig. 7). In general, the concentration-response curves for the inhibitions of RNA and protein syntheses by **PQ1** are similar to that for its inhibition of DNA synthesis: concentrations of **PQ1** >10 μM have to be used to demonstrate effectiveness and maximal inhibition is achieved at 25 μM. Under similar conditions, Mitox and 17-AAG inhibit RNA synthesis to a greater degree than **PQ1**, whereas radicicol is slightly less effective (Fig. 7A). For the inhibition of protein synthesis, Mitox and radicicol are more effective than **PQ1** but 17-AAG is much weaker and fails to inhibit this response by more than 50% even at the highest concentration tested (Fig. 7B).

DNA binding and fragmentation. High concentrations of antiproliferative **PQ1** and reference anticancer drugs were evaluated for their DNA-binding affinity in a cell-free system, using the classic EB displacement assay to identify intercalating or non-intercalating drugs that destabilize the DNA double helix. Whether administered as pre- or post-treatments, 20-125 μM concentrations of **PQ1** or radicicol do not induce a loss of EB fluorescence, suggesting that these antiproliferative compounds do not directly interact with double-stranded ct DNA to disrupt its structural and functional integrity and prevent the dye from intercalating into DNA base pairs (Fig. 8). In contrast, positive controls of 1.28-8 μM Mitox, which destabilize double-stranded ct DNA to prevent or disrupt EB intercalation, almost totally suppress (inhibition by 53-95%) the fluorescence of the EB-DNA complex (Fig. 8). Under these experimental conditions, the concentration-dependent inhibition of EB binding to DNA by Mitox has an IC_{50} of 1.2 μM (data not shown). On an equimolar concentration basis, the DNA-binding activity of 20-125 μM 17-AAG, which inhibits the fluorescence of the EB-DNA complex by 34-68%, is much weaker than that of Mitox but suggests that the ability of this anticancer drug to directly interact with DNA may also play a role in its mechanism of action (Fig. 8).

The ability of **PQ1** to induce internucleosomal DNA fragmentation at 24 h was assessed and compared to those of 17-AAG, radicicol and Mitox by two different techniques, using L1210 cells containing [^{3}H]-thymidine-prelabeled DNA to detect low molecular weight DNA fragments after intact chromatin precipitation (Fig. 9) or agarose gel electrophoresis

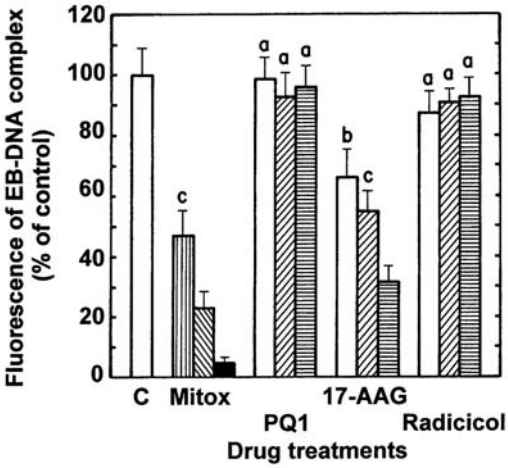

Figure 8. Comparison of the abilities of 1.28 (vertical stripes), 3.2 (diagonale stripes) or 8 μM (solid column) Mitox and 20 (open columns), 50 (diagonale stripes) or 125 μM (horizontal stripes) concentrations of **PQ1**, 17-AAG and radicicol to inhibit the binding of EB to double-stranded ct DNA. Results were expressed as % of the control (C) fluorescence of the EB-DNA complex in the absence of drug at 525 nm excitation and 600 nm emission (159.8±14.1 AU; 100±8.8%). The background of EB fluorescence in the absence of DNA was subtracted from the results (26.2±2.3 AU). Bars, means ± SD (n=3). [a]Not different from control; [b]P<0.025 and [c]P<0.005, smaller than control.

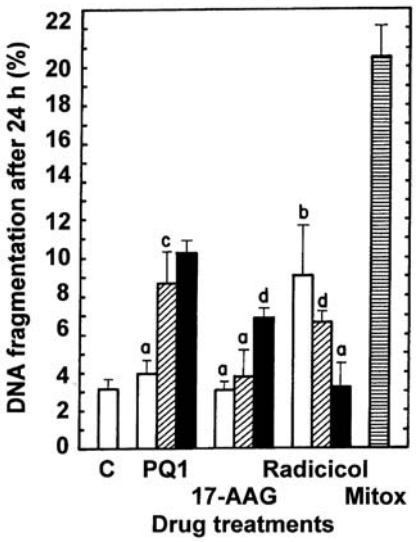

Figure 9. Comparison of the abilities of 4 (open columns), 10 (diagonale stripes) and 25 μM (closed columns) concentrations of **PQ1**, 17-AAG and radicicol to induce DNA fragmentation at 24 h in L1210 cells containing [^{3}H]-prelabeled DNA *in vitro*. The level of DNA fragmentation caused by 256 nM Mitox (horizontal stripes) was used as a positive control. The results were expressed as [cpm in supernatant/cpm in supernatant + pellet] x 100 at 24 h. For untreated control (C) tumor cells (3.23±0.46% DNA fragmentation), the supernatant (DNA fragments) was 4,581±661 cpm and the pellet (intact DNA) was 137,260±19,271 cpm. Bars, means ± SD (n=3). [a]Not different from control; [b]P<0.025, [c]P<0.01 and [d]P<0.005, greater than control.

to visualize the typical pattern of DNA laddering indicative of apoptosis (Fig. 10). As compared to untreated controls (3.2% DNA fragmentation), 25 μM **PQ1**, 25 μM 17-AAG and 4 μM radicicol respectively induce 3.2-, 2.1- and 2.8-fold increases in the level of DNA cleavage in L1210 cells at 24 h (Fig. 9). The fact that a higher 6.4-fold stimulation of DNA fragmentation is achieved by a 256 nM concentration of Mitox 15.6 times lower than that of radicicol and 97.7 times lower than that of **PQ1** suggests that this anticancer drug is more cytotoxic than the above compounds (Fig. 9). The ability of **PQ1** to induce internucleosomal fragmentation was confirmed by agarose gel electrophoresis of DNA samples extracted after 24 h from L1210 cells treated with increasing concentrations of this antiproliferative compound (Fig. 10). Compared to untreated control, DNA cleavage bands with a characteristic pattern of internucleosomal ladders become increasingly visible in response to 1.6-25 μM concentrations of **PQ1** (Fig. 10). Again, on an equimolar concentration basis, 256 nM Mitox is a more potent inducer of internucleosomal DNA fragmentation than 4 μM radicicol and 25 μM **PQ1** or 17-AAG, based on the greater intensity of the bands of DNA laddering extracted from Mitox-treated L1210 cell samples at 24 h (Fig. 10).

Mitotic index and abnormalities. Control populations of L1210 cells cultured for 24 h in the absence of drugs contain only 0.46% of mitotic cells (Table I). In relation with their ability to disrupt microtubule dynamics, 24-h treatments with VCR, which blocks tubulin polymerization and microtubule assembly, and taxol, which lowers the critical concentration of free tubulin required to promote polymerization and blocks microtubule disassembly, respectively produce 25.7- and 8.2-fold increases in the mitotic index (Table I). Such microtubule de-stabilizing and stabilizing anticancer drugs known to block cell cycle progression in M-phase, therefore, served as positive controls in this antimitotic assay. Under similar conditions, antiproliferative concentrations of **PQ1** 40-100 times greater than those of VCR and taxol produce weak 2.0- to 2.5-fold increases in the mitotic index of L1210 tumor cells at 24 h but stimulate the formation of many binucleated cells (3.2- to 7.4-fold increases) and a few micronuclei, suggesting that this compound might enhance mitotic abnormality, induce chromosomal damage or missegregation, and block cytokinesis (Table I). In the same experiments, microtubule de-stabilizing VCR prevents the formation and lowers the % of binucleated cells below the background level observed in untreated control cells, whereas microtubule-stabilizing taxol produces large increases in the incidence of cells containing 2 nuclei (6.8-fold stimulation) or micronuclei (8.4-fold stimulation) (Table I). This is in agreement with the fact that taxol-treated cells with stabilized spindle microtubules escape from mitosis without cytokinesis and proceed as binucleated cells to the next round of DNA synthesis to form polynucleated polyploid cells which eventally die (22).

Induction of PARP-1 cleavage and activation of initiator and effector caspases. **PQ1**, 17-AAG and radicicol treatments that induce internucleosomal DNA fragmentation in L1210 cells at 24 h were tested for their ability to induce PARP-1 cleavage, an early marker of apoptosis characterized by the disappearance of the 116-kDa band of the native enzyme. No or very little PARP-1 cleavage is detected in untreated control cells but the band of the 85-kDa fragment becomes increasingly apparent 1-4.5 h after treatment of L1210 cells

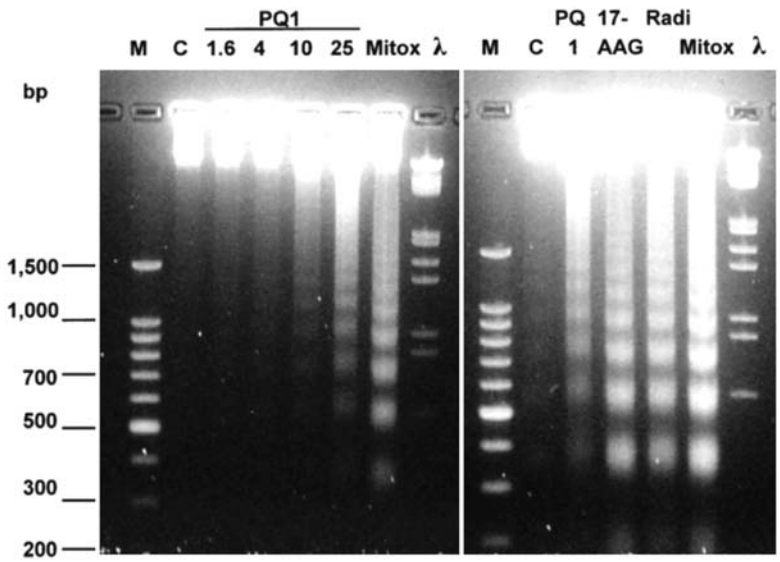

Figure 10. Agarose gel analysis of drug-induced internucleosomal DNA fragmentation in L1210 cells *in vitro*. Left, concentration-dependent levels of DNA fragmentation in cells incubated at 37˚C for 24 h in the presence or absence (control, lane C) of 1.6, 4, 10 or 25 μM **PQ1** and 256 nM Mitox. Right, levels of DNA fragmentation in cells incubated at 37˚C for 24 h in the presence or absence (control, lane C) of 25 μM **PQ1**, 25 μM 17-AAG, 4 μM radicicol and 256 nM Mitox. Cellular DNA extracts (6 μg/well) were loaded onto a 1.5% agarose gel containing EB (1 μg/ml), separated by electrophoresis for 3.7 h at 60 V and photographed under UV light. A typical ladder pattern indicating the presence of DNA equivalent to the size of single and oligo nucleosomes is characteristic of apoptosis. Size markers are shown in lanes M (0.5 μg of 100 bp standard DNA ladder) and λ (0.75 μg of lambda DNA/*Eco*RI + *Hin*dIII markers).

Table I. Effects of novel substituted quinoline on the mitotic index and the frequencies of binucleated cells and micronuclei in L1210 tumor cells *in vitro*.

Compounds (code no.)[a]	Mitotic cells (%)[b]	Mitotic index[c]	Binucleated cells (%)[b]	Binucleated cell index[c]	Cells with micronuclei (%)[b]
Control	0.46±0.11	-	1.52±0.42	-	0
PQ1 (0.64 μM)	0.31±0.09[d]	0.67	4.26±0.41[g]	2.80	0.10±0.03
PQ1 (1.6 μM)	0.72±0.14[d]	1.57	4.35±1.02[f]	2.86	0.09±0.02
PQ1 (4 μM)	0.90±0.25[e]	1.96	4.82±0.47[g]	3.17	0.12±0.05
PQ1 (10 μM)	1.17±0.33[f]	2.54	11.23±1.40	7.39	0.28±0.13
VCR (0.1 μM)	11.84±1.51	25.74	0.39±0.16[h]	0.26	0.16±0.02
Taxol (0.1 μM)	3.79±1.44	8.24	10.39±1.01	6.84	8.36±1.70

[a]L1210 cells were incubated in triplicate for 24 h at 37˚C in the presence or absence (control) of the indicated concentrations of drugs. [b]The % of cells in each category was determined by morphologic analysis, scoring at least 2,000 cells/slide to identify those containing mitotic figures, 2 nuclei or micronuclei. Means ± SD (n=3). [c]Percentage of mitotic or binucleated cells in drug-treated cultures divided by the % of mitotic or binucleated cells in vehicle-treated controls. [d]Not different from control; [e]P<0.05, [f]P<0.025 and [g]P<0.005, greater than control; [h]P<0.025, smaller than control.

with 25 μM **PQ1** (Fig. 11). 17-AAG and radicicol are inactive at 1-4.5 h and longer incubation times are required to detect the induction of PARP-1 cleavage by these antitumor drugs (Fig. 11). In contrast to necrotic cells, which contain large amounts of uncleaved PARP-1 (23), virtually no intact PARP-1 is left after 20 h in apoptotic cells treated with 4 μM radicicol, as indicated by the nearly total disappearance of the 116-kDa band of the native enzyme (Fig. 11). However, PARP-1 is only partially cleaved by 25 μM **PQ1** at 3-4.5 h and 10 μM 17-AAG at 20 h, based on the substantial intensity of the 116-kDa remnant and the smaller band of the 85-kDa fragment (Fig. 11). Overall, the results suggest that antiproliferative **PQ1**, 17-AAG and radicicol are weak and/or slow inducers of apoptotic PARP-1 cleavage and internucleosomal DNA fragmentation.

Since the degradation of PARP-1 is catalyzed by caspase-3, the **PQ1** treatments shown to induce PARP-1 cleavage and internucleosomal DNA fragmentation were tested for their

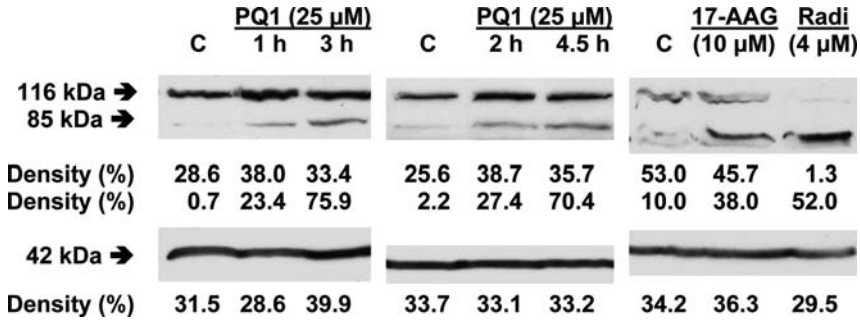

Figure 11. Determination of drug-induced PARP-1 cleavage in L1210 cells *in vitro*. Tumor cells were incubated for 1-4.5 h in the presence or absence (control, lane C) of 25 μM **PQ1** and for 20 h in the presence or absence (control, lane C) of 10 μM 17-AAG or 4 μM radicicol and bands (arrows) of intact (M_r ~116,000) and cleaved (M_r ~85,000) PARP-1 were detected by Western blot analysis. Coimmunodetection of ß-actin bands (M_r ~42,000) was performed on the same membranes to confirm equal protein loading in each lane. The relative band densities in equal areas are expressed as the % that each box contributed to the total density measured after automatic background correction.

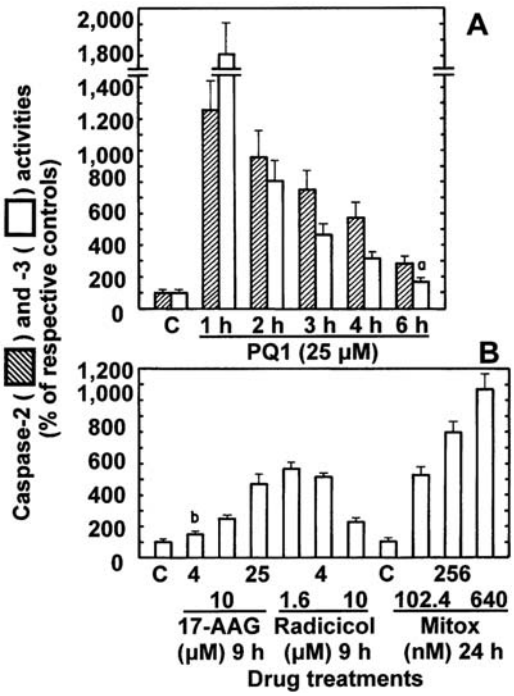

Figure 12. Fluorogenic assay of initiator and effector caspase activation in drug-treated L1210 cells *in vitro*. (A) Comparison of the time-dependent inductions of caspase-2- (striped columns) and caspase-3-like (open columns) protease activities in L1210 cells incubated for 1-6 h in the presence or absence (C, control) of 25 μM **PQ1** *in vitro*. The results are respectively expressed as % of VDVAD (5.6±0.6 nmol AFC released/mg protein, 100±9.9%, striped control) or % of DEVD (11.9±0.8 nmol AFC released/mg protein, 100±6.9%, open control) cleavage activities in vehicle-treated control tumor cells at 1-6 h. Bars, means ± SD (n=3). (B) Comparison of the concentration-dependent inductions of caspase-3-like protease activity in L1210 cells incubated for 9 h in the presence or absence (C, control) of 17-AAG or radicicol and for 24 h in the presence or absence (C, control) of Mitox. The results are respectively expressed as % of DEVD cleavage activities in vehicle-treated control tumor cells at 9 (10.7±0.9 nmol AFC released/mg protein, 100±8.1%) and 24 h (24.1±1.2 nmol AFC released/mg protein, 100±4.8%). $^{a}P<0.01$ and $^{b}P<0.005$, greater than respective controls.

ability to activate this key post-mitochondrial effector caspase. Caspase-2 activity was also assayed because stimulation of this apical caspase may be required to activate the downstream cascade of other initiator and effector caspases in drug-treated tumor cells (16,18). The hypothesis that the caspase activation cascade is involved in PARP-1 cleavage by **PQ1** at 1-4.5 h (Fig. 11) is substantiated by the fact that caspase-2 (1,258% of the control) and -3 (1,810 % of the control) activities are all maximally induced in L1210 cells as early as 1 h after treatment with 25 μM **PQ1** (Fig. 12). Interestingly, the concentration-dependent abilities of 17-AAG, radicicol and Mitox to maximally induce caspase-3 activity in L1210 cells at 9 or 24 h (Fig. 12) resemble the inductions of internucleosomal DNA fragmentation caused by these drugs at 24 h (Figs. 9 and 10), 17-AAG being the most effective activator of caspase-3 at concentrations increasing toward 25 μM (468% of the control), radicicol at concentrations decreasing toward 4-1.6 μM (515-570% of the control), and Mitox at even lower 256-640 nM concentrations (798-1,068% of the control (Fig. 12).

HER1 and HER2 protein level and autophosphorylation. Small molecules that interact with and inactivate the human EGF receptors HER1 and HER2, and/or their Hsp90 chaperone, might effectively block the aberrant ligand-dependent and -independent signaling pathways that sustain the proliferation of various HER1- and HER2-overexpressing tumor cell lines (24). After inhibition of their Hsp90 chaperone, destabilized HER1 and HER2 client proteins generally undergo proteosomal degradation (25,26). Indeed, whole cell immunodetection confirms that the known Hsp90 inhibitors 17-AAG and radicicol (21,27) downregulate, in a concentration-dependent manner, HER1 protein level in A-431 cells and HER2 protein level in SK-BR-3 cells, receptor degradation after 24 h being significant at 41 or 102 nM and maximal or near maximal at 256 or 640-1,600 nM (Fig. 13). In contrast, none of the concentrations of antiproliferative **PQ1** tested up to 25 μM altered HER1 and HER2 protein levels in these A-431 and SK-BR-3 tumor cells after 24 h, suggesting that this drug is unlikely to inhibit Hsp90 to destabilize the HER1- and HER2-mediated signal transduction pathways (Fig. 13). As HER1 and HER2 receptor tyrosine kinases are activated by oligomerization and autophosphorylation (24,28), it was of interest to determine whether **PQ1** would reduce the levels of pHER1 in EGF-stimulated A-431 cells and pHER2 in SK-BR-3 cells after 3 h. Because the primary event in signaling after HER1 and HER2 oligomerization is autophosphorylation, inhibition of receptor autophosphory-

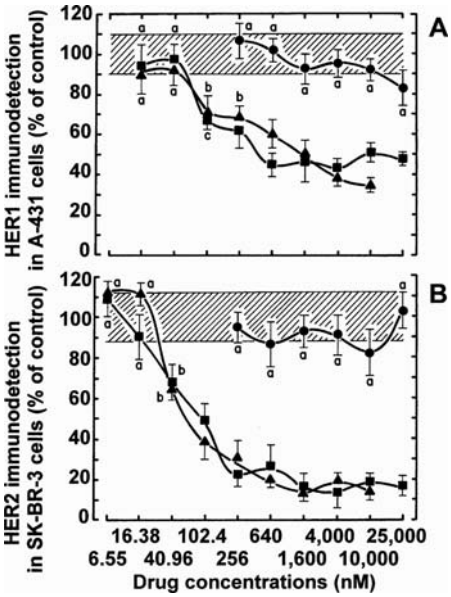

Figure 13. Whole cell immunodetection of HER1 (A) and HER2 (B) protein levels *in vitro*. Comparison of the abilities of serial concentrations (logarithmic scale) of **PQ1** (●), 17-AAG (■) and radicicol (▲) to induce HER1 degradation in A-431 cells (A) and HER2 degradation in SK-BR-3 cells (B) at 24 h. The results are respectively expressed as % of the ratios of HER1 or HER2 protein levels (relative luminescence intensity of the anti-HER1 or anti-HER2 primary antibody-antigen immune complexes bound to horseradish peroxidase-linked secondary antibody):cell numbers (relative fluorescence intensity of Hoechst reagent-DNA complexes) in vehicle-treated control A-431 (0.0194±0.0019, 100±10%, striped area in A) or SK-BR-3 cells (0.0397±0.0048, 100±12%, striped area in B) at 24 h. Bars, means ± SD (n=3). [a]Not different from respective controls; [b]P<0.025 and [c]P<0.01, smaller than respective controls.

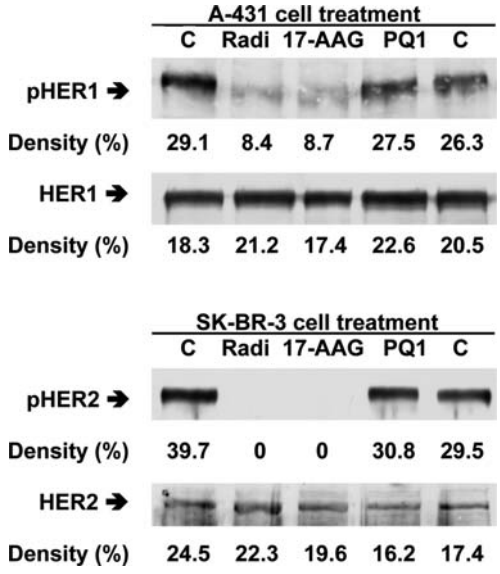

Figure 14. Comparison of the abilities of **PQ1**, 17-AAG and radicicol to inhibit HER1 and HER2 receptor phosphorylation in A-431 and SK-BR-3 cells, respectively. Tumor cells were incubated for 3 h in the presence or absence (control, lanes C) of 4 μM radicicol and 17-AAG or 25 μM **PQ1**. HER1-overexpressing A-431 cells were stimulated with EGF for the last 15 min of incubation. The phosphorylation states of HER1 and HER2 were respectively analyzed by Western blotting with anti-pHER1 and anti-pHER2 antibodies. In the same experiments, membranes were also probed with anti-HER1 or anti-HER2 antibodies to quantitate receptor protein loading in each lane. The relative band densities in equal areas are expressed as the % that each box contributed to the total density measured after automatic background correction.

lation is an indicator of compound potency and selectivity (29,30). Again, Western blot analysis indicates that, on an equal HER1 and HER2 protein level basis, 25 μM **PQ1** does not mimic the ability of 4 μM 17-AAG and radicicol to suppress the levels of pHER1 and pHER2 respectively detected in A-431 and SK-BR-3 cells at 3 h (Fig. 14). The results indirectly suggest that **PQ1** does not target Hsp90 or HER1 and HER2 receptor kinases to inhibit tumor cell proliferation and trigger apoptosis.

Discussion

Quinolines, which induce anti-malarial, leishmanicidal, antibacterial and anticancer activities, have been reported to inhibit ATP-binding cassette drug transporter, tumor hypoxia, multidrug resistance (MDR) and protein tyrosine kinase activity (reviewed in ref. 1). The present study demonstrates that substituted quinoline **PQ1**, previously shown to inhibit the viability of T-47D human breast cancer cells and their ability to grow colonies on soft agar *in vitro* and form xenograft tumors in nude mice *in vivo* (1,2), is also consistently effective against tumor cell proliferation in the low μM range in a small panel of leukemic, pancreatic, epidermoid and mammary tumor cells. The fact that antitumor **PQ1** is effective in the nM range in the T-47D cell system (1,2) is substantiated by the present data showing that 200 nM **PQ1** can inhibit the Ki-67 marker of cell proliferation in these T-47D tumor cells. Although the magnitudes of inhibition may vary and **PQ1** may be more effective against T-47D than L1210 cells, the MTS:PMS assay of metabolic activity at 2 and 4 days, the trypan blue exclusion test of membrane integrity at 2 days (1), the MTT assay at day 1 and the colony growth assay at 7 days (2) all concord to demonstrate that **PQ1** is a potent antitumor agent that inhibits the proliferation, viability and reproductive ability of various tumor cells. **PQ1** is the most effective antipoliferative agent among the PQ analogs tested in the L1210 cell system but **PQ11** has the strongest antiproliferative activity in the T-47D cell system (1), suggesting that these synthetic substituted quinolines might selectively inhibit the growth of certain mammary tumor cell lines in the nM range. The results are encouraging given the fact that strong anticancer compounds were discovered among only a handful of PQ analogs synthesized. The antitumor activities of **PQ1** open the possibility of designing new anticancer drugs based on this framework. **PQ1** possesses an aminopropyl side chain at C9 amine function of the quinoline ring, which is likely to enhance its ability to interact with various molecular targets in the cells.

The Ki-67 protein, which is absent from resting cells (G_0), can be exclusively detected within the nuclei of cells progressing through the G_1, S and G_2 phases of the cell cycle and relocates to the surface of the chromosomes during mitosis (11). Because Ki-67 expression may be absolutely required to maintain tumor cell proliferation, the fraction of Ki-67-positive tumor cells is often correlated with the clinical course of cancer (11). Hence, it is significant to show that a nM concentration of **PQ1** can dramatically inhibit the expression of Ki-67 antigen for at least 48 h, suggesting that this novel antitumor compound might be effective for reducing the growth fraction of tumor cell populations and controlling disease progression. The observation that some

PQ1-treated tumor cells resumed expressing the Ki-67 antigen at 72 h might be due to the partial degradation of the drug producing inactive metabolites. Further pharmacokinetic studies would be required to assess the half-life, cellular uptake, retention and intracellular distribution of PQ compounds and evaluate their duration of action.

In accordance with the effects of established anticancer drugs used as positive controls, concentrations of **PQ1** higher than those sufficient to inhibit tumor cell proliferation must be used to inhibit nucleoside transport and macromolecule syntheses or maximally induce caspase activities, PARP-1 cleavage and apoptotic DNA fragmentation. Such apparent discrepancy may simply be due to different experimental conditions and cellular responses to various periods of drug exposure: the cellular uptakes of purine and pyrimidine nucleosides over 30 sec are blocked in cells treated for only 15 min with **PQ1** and 17-AAG, the rates of nucleic acid and protein syntheses over 30-60 min are inhibited in cells treated for only 2-3 h with **PQ1**, Mitox, 17-AAG or radicicol, caspase activation and PARP-1 cleavage are induced in cells treated for only 1-4.5 h with **PQ1**, 9-20 h with 17-AAG or radicicol and 24 h with Mitox, and maximal internucleosomal DNA fragmentation occurs 24 h after anticancer drug treatment, whereas the more spectacular inhibitions of L1210, Pan02, A-431, SK-BR-3 and BT-474 tumor cell proliferation are the result of 2- to 4-day long drug treatments. Although synthetic **PQ1** is weaker than established anticancer drugs like DAU, Mitox, 17-AAG and radicicol, the interest with this small molecule may be its novel molecular targets and mechanisms of antitumor activity, based on the observation that **PQ1** may be the 1st compound that can interact with gap junction and decrease Cx43 phosphorylation to specifically restore GJIC and inhibit cell proliferation in tumor rather than normal tissues (2). The molecular mechanism by which **PQ1** restores GJIC in tumor cells (1,2) is under investigation. One hypothesis is that **PQ1** may prevent the degradation of Cx43 (3) by interacting with E3 ubiquitin ligase. **PQ1** might block the interaction between the PY motif of Cx43 and the WW domain of E3 ubiquitin ligase.

PQ1 mimics the ability of Mitox, radicicol and 17-AAG to inhibit DNA, RNA and protein syntheses in L1210 tumor cells but, in contrast to inactive Mitox and radicicol, has the additional advantage of targeting the nucleoside transport system to rapidly block the cellular uptake of purine and pyrimidine nucleosides. Hence, **PQ1** may disrupt other cell membrane targets besides gap junctions and its ability to block within 15 min the cellular uptake of [^{3}H]-adenosine and [^{3}H]-thymidine is likely to play a role in the mechanism by which this compound inhibits after 2-3 h the rates of incorporation of purines and pyrimidine nucleosides required for nucleic acid syntheses. Radicicol (25-62.5 μM) and Mitox (1.6-4 μM) are totally unable to alter the cellular transport of [^{3}H]-adenosine and [^{3}H]-thymidine even though these drugs at such concentrations inhibit maximally the incorporation of [^{3}H]-thymidine into DNA. Interestingly, 17-AAG also inhibits nucleoside transport suggesting that Hsp90 inhibition may not be the sole molecular target of its mechanism of antitumor activity.

For nucleotide synthesis, cells use purine and pyrimidine nucleosides generated either through *de novo* synthesis or through salvage pathways for the re-utilization of pre-existing nucleobases. L1210 cells possess 3 distinct types of nucleoside transporters that function by equilibrative (facilitated diffusion) or Na^+-dependent (concentrative) mechanisms and are either sensitive or insensitive to specific nucleoside transport inhibitors (reviewed in ref. 31 and refs. therein). The direct interaction of **PQ1** with nucleoside transporters remains to be determined but these molecular targets might be valuable in polychemotherapy to potentiate the anticancer action of antimetabolites since tumor cells might up-regulate their nucleoside transport system to compensate for the inhibitory effects of antimetabolites on nucleic acid syntheses. MDR is sometimes associated with increases in the number of nucleoside transporters and their rate of transport, resulting in the increased uptake of adenosine and nucleoside salvage pathway that limit the efficacy of methotrexate and 5-fluorouracil. By blocking the rescue effect of exogenous nucleosides, nucleoside transport inhibitors may potentiate or prolong the anticancer activity of antimetabolites which inhibit the *de novo* pathway for nucleotide synthesis (reviewed in ref. 15 and refs. therein). Moreover, nucleoside transport inhibitors may also circumvent DAU resistance by interfering with both P-glycoprotein and nucleoside transport in MDR cells (15,31). Hence, **PQ1** might also be valuable to circumvent some of the mechanisms of MDR and sensitize MDR tumor cells that have become unresponsive to the cytotoxicity of conventional DNA-damaging anticancer drugs.

FDA-approved Mitox is a synthetic anthracenedione related to DAU but less cardiotoxic. Besides targeting the DNA topoisomerase II enzyme to induce DNA damage, the mechanism of action of anthracycline-type antitumor drugs involves intercalation of the planar aglycone moiety into DNA to disrupt DNA replication and transcription (32). Hence, the present EB results are consistent with the fact that Mitox (1.28-8 μM) is a DNA-reactive agent that intercalates into DNA and causes crosslinks and strand breaks. Apparently, higher 20-125 μM concentrations of 17-AAG can also bind to purified DNA to disrupt the EB-DNA complex, suggesting that some level of DNA damage may play a role in the mechanism of action of this anticancer drug. But this is not the case for **PQ1** and radicicol, suggesting that these drugs, which do not directly bind to DNA to inhibit the fluorescence of the EB-DNA complex in a cell-free assay, are unlikely to directly target cellular DNA to exert their antitumor activities.

The inability of **PQ1** to substantially raise the mitotic index of L1210 cells like VCR and taxol do at 24 h suggests that this compound is not a mitotic spindle poison and unlikely to interact with tubulin and alter the polymerization/depolymerization of microtubules in order to elicit its antiproliferative activity. But increasingly antiproliferative 0.64-10 μM concentrations of **PQ1** might trigger some genotoxic effects to increase the levels of binucleated cells and micronuclei in L1210 tumor cells at 24 h. Binucleated cells indicate that cytokinesis is inhibited following nuclear division (19). Multinucleated cells may follow if binucleated cells re-enter the cell cycle and escape further cytokinesis. The micronucleus test is an indicator of drug-induced chromosomal damage and aberration as such structures generally form during the metaphase/anaphase transition of mitosis when a whole lagging chromosome or an acentric chromosome fragment

resulting from a clastogenic or mutagenic event fail to integrate into the daughter nuclei (19). However, chromosome aberration and non-disjunction/missegregation might be the consequence of prolonged drug-induced mitotic disruption and might be responsible for cellular inability to undergo cytokinesis after regression of the cleavage furrow (33). If completion of cytokinesis requires accurate chromosome segregation, it is possible that **PQ1** treatment induces chromosome aberration and missegregation to increase the frequency of binucleated cells.

In contrast to the early cleavage of DNA into large 50-300 kbp fragments, an initial signaling event that may induce tumor cells treated with relatively low concentrations of DNA-damaging anticancer drugs to commit apoptosis, the secondary endonucleolytic degradation of DNA at internucleosomal linker sites to produce small 180-200 bp mono- and oligonucleosomal fragments at 24 h is a late marker concurrent with morphological evidence of apoptosis (34). Upstream of internucleosomal DNA fragmentation, activation of the caspase cascade induces the proteolytic cleavage of a wide range of substrates. Effector caspase-3 cleaves and inactivates the inhibitor of caspase-activated DNase, thus releasing active endonucleases that translocate into the nucleus to achieve internucleosomal DNA fragmentation (34). The caspase-3-mediated cleavage and inactivation of PARP-1 is also an early event required for tumor cells that have been exposed to DNA-damaging anticancer drugs and have entered the process of apoptosis. PARP-1 cleavage may prevent the detection and repair of DNA damage, block the depletion of NAD^+ and ATP causing necrotic cell death, and enhance the activity of Ca^{2+}/Mg^{2+}-dependent endonucleases (23,35). For this reason, detection of the disappearance of the native 116-kDa enzyme and appearance of the 85-kDa fragment of PARP-1 cleavage is an early and sensitive indicator that L1210 cells treated with **PQ1** or reference anticancer drugs used as positive controls are undergoing apoptosis (18,20). The present data indicate that concentrations of **PQ1**, which block nucleoside transport at 15 min and macromolecule syntheses within 2-3 h, stimulate an apoptotic pathway that induces a cascade of initiator caspase-2 and effector caspase-3 activations at 1 h and PARP-1 cleavage at 1-4.5 h in relation with their ability to disrupt cytokinesis and trigger internucleosomal DNA fragmentation at 24 h and inhibit tumor cell proliferation over a 2-4-day period, suggesting that the ability of this substituted quinoline to induce apoptosis may play a significant role in its molecular mechanism of action.

Whether extrinsic or intrinsic pathways are involved, all apoptotic pathways eventually converge on the mitochondrial outer membrane where the activation of proapoptotic Bcl-2 family members causes mitochondrial permeability transition (MPT) and the release of apoptogenic factors (16,18,34,36). DNA-damaging anticancer drugs are believed to trigger an intrinsic mitochondrial-dependent pathway in which nuclear signals that involve various p53-responsive genes directly induce the Bax- and Bak-mediated opening of the mitochondrial pores and the release of cytochrome *c* (Cyt *c*) from the intermembrane space into the cytosol that is the key limiting factor in initiating the postmitochondrial cascade of apoptotic proteases (34,37). Cyt *c* binds to apoptotic protease-activating factor-1, which interacts with procaspase-9 to form the apoptosome complex that activates this initiator caspase in the presence of dATP (37). In drug-treated HL-60 cells, the critical release of mitochondrial Cyt *c* can fully occur in the absence of apical caspase activation, suggesting that Cyt *c* release is an upstream and caspase-independent event in drug-induced apoptosis (18,36). But a specific caspase-2 inhibitor blocks caspase-9, -3 and -8 activations in drug-treated HL-60 cells, demonstrating that apical caspase-2 may be activated upstream of the other initiator and effector caspases and control their subsequent activations (18,36). Even though **PQ1** does not directly bind to DNA, the abilities of this antitumor compound to interact with maintenance enzymes or regulatory proteins and indirectly cause high molecular weight DNA-strand breaks, crosslinks or chromosome aberrations and cytokinesis disruption remain to be determined. Therefore, it is rather premature to speculate on the nature of the primary molecular targets, massive damaging events and nuclear signals that induce **PQ1**-treated tumor cells to release their mitochondrial Cyt *c* and undergo apoptosis, thereby activating their postmitochondrial caspase cascade responsible for PARP-1 cleavage, endonuclease activation and, ultimately, the internucleosomal fragmentation of their DNA, which is one of the late manifestations of the apoptotic process. Markers of MPT linked to the sudden increase in the permeability of the inner membrane include the collapse of mitochondrial transmembrane potential ($\Delta\Psi_m$), large amplitude swelling and Ca^{2+} release (reviewed in refs. 38,39 and refs. therein). Cyt *c* release is a universal event in apoptosis but this can occur before, independently or in the absence of collapse of $\Delta\Psi_m$, and without concomitant opening of mitochondrial permeability transition pores (PTP) and swelling (38,39). In contrast to antitumor triptycene and 1,4-anthracenedione analogs (38,39), **PQ1** causes neither the collapse of $\Delta\Psi_m$, mitochondrial swelling nor Ca^{2+} release in cell and cell-free systems (data not shown), suggesting that this compound is unlikely to target mitochondria to induce Cyt *c* release, either directly, through conformational changes that disrupt the open-closed transition of the PTP complex (40), or indirectly, through sequential DNA damage and early PARP-1 activation resulting in mitochondrial NAD^+ depletion and dysfunction (41). Like most of the current anticancer drugs, **PQ1** does not have the option of directly targeting mitochondria but must first damage other molecular targets in order to generate the signals that trigger the mitochondrial pathway of apoptosis.

17-AAG, a less toxic analog of the ansamycin antibiotic geldanamycin, and the macrolide radicicol are potent inhibitors of Hsp90, a molecular chaperone whose association is required for the posttranslational folding, stability and function of multiple mutated, chimeric, and overexpressed signaling proteins that promote cancer cell growth and/or survival (42). As a significant number of tumors express increased levels of active Hsp90 and HER1 and HER2 client proteins, one approach to inhibiting multiple signal transduction pathways with one agent, is to block the ATP-binding site of Hsp90 (43). By inhibiting Hsp90 function, 17-AAG and radicicol cause the selective proteosomal degradation of several oncogenic membrane receptor and intracellular protein tyrosine kinases that regulate multiple signaling pathways for tumor cell proliferation, cell cycle regulation, cell survival, invasion, metastasis and angiogenesis, and thus induce apoptosis and antitumor effects (21,25-27). In contrast to bulky and

highly specific mAbs, small multikinase inhibitors that target both HER1 and HER2 receptors might be advantageous to block multiple steps along different receptor tyrosine kinase signaling networks and inhibit the growth of a broader range of neoplastic cells (24,28-30). Since **PQ1** fails to mimic the abilities of 17-AAG and radicicol to drastically reduce the protein level and phosphorylation status of ligand-dependent HER1 in HER1-overexpressing A-431 cells and ligand-independent HER2 in SK-BR-3 cells, this new drug is unlikely to target Hsp90 and downregulate or inactivate client onco-proteins of the EGF signaling pathway to inhibit tumor cell growth and promote apoptosis.

Combining drugs that target different molecular pathways and achieve complementary or synergistic antitumor effects is an important strategy in cancer chemotherapy. **PQ1**, which targets gap junctions (2) and decreases Ki-67 expression in the nM range and also inhibits nucleoside transport, blocks cytokinesis and induces apoptotic DNA fragmentation in the μM range, might disrupt a wider spectrum of molecular targets in populations of unsynchronized tumor cells and have a more versatile mechanism of action than another drug affecting a single of these events. The inability of **PQ1** to reduce the protein level and phosphorylation of EGF receptors in tumor cell membranes reinforces the notion that the enhancement of GJIC (2) plays a major role in its mechanism of antitumor activity.

Acknowledgements

This study was supported in part by grants from the Howard Hughes Medical Institute (Biological Sciences Education Grant), Kansas State University (Innovative Research Award from the Terry C. Johnson Center for Basic Cancer Research and Research Seed Grant Award from the Biology Research and Instruction Enhancement Fund Program), and the National Institutes of Health (AG025500 and NIH-COBRE P20RR017686).

References

1. Shi A, Nguyen TA, Battina SK, Rana S, Takemoto DJ, Chiang PK and Hua DH: Synthesis and anti-breast cancer activities of substituted quinolines. Bioorg Med Chem Lett 18: 3364-3368, 2008.
2. Gakhar G, Ohira T, Shi A, Hua DH and Nguyen TA: Antitumor effect of substituted quinolines in breast cancer cells. Drug Dev Res 69: 526-534, 2008.
3. Musil LS, Le AC, van Slyke JK and Roberts LM: Regulation of connexin degradation as a mechanism to increase gap junction. J Biol Chem 275: 25207-25215, 2000.
4. Martin PE and Evans WH: Incorporation of connexins into plasma membranes and gap junctions. Cardiovasc Res 62: 378-387, 2004.
5. Ruch RJ: The role of gap junctional intercellular communication in neoplasia. Ann Clin Lab Sci 24: 216-231, 1994.
6. Zhang ZQ, Lin ZX and Lu YY: Studies on the reduction of malignant phenotypes in a highly metastatic human lung carcinoma - correlated changes of intercellular communication, cytoskeletons, oncogenes and antioncogenes. Zhonghua Zhong Liu Za Zhi (Chin J Oncol) 16: 88-92, 1994.
7. Na HK, Wilson MR, Kang KS, Chang CC, Grunberger D and Trosko JE: Restoration of gap junctional intercellular communication by caffeic acid phenethyl ester (CAPE) in a ras-transformed rat liver epithelial cell line. Cancer Lett 157: 31-38, 2000.
8. Holder JW, Elmore E and Barrett JC: Gap junction function and cancer. Cancer Res 53: 3475-3485, 1993.
9. Dubina MV, Iatckii NA, Popov DE, Vasil'ev SV and Krutovskikh VA: Connexin 43, but not connexin 32, is mutated at advanced stages of human sporadic colon cancer. Oncogene 21: 4992-4996, 2002.
10. Eghbali B, Kessler JA, Reid LM, Roy C and Spray DC: Involvement of gap junctions in tumorigenesis: transfection of tumor cells with connexin 32 cDNA retards growth *in vivo*. Proc Natl Acad Sci USA 88: 10701-10705, 1991.
11. Scholzen T and Gerdes J: The Ki-67 protein: from the known and the unknown. J Cell Physiol 182: 311-322, 2000.
12. Lauer WMRC, Arnold RT, Drake NL, Hook JV and Tinker J: Some derivatives of 8-aminoquinoline. J Am Chem Soc 68: 1546-1548, 1946.
13. LaMontagne MP, Blumberg P and Strube RE: Antimalarials. 14. 5-(Aryloxy)-4-methylprimaquine analogues. A highly effective series of blood and tissue schizonticidal agents. J Med Chem 25: 1094-1097, 1982.
14. Cory AH, Owen JC, Barltrop JA and Cory JG: Use of an aqueous soluble tetrazolium/formazan assay for cell growth assays in culture. Cancer Commun 3: 207-212, 1991.
15. Perchellet EM, Magill MJ, Huang X, Dalke DM, Hua DH and Perchellet J-P: 1,4-Anthraquinone: an anticancer drug that blocks nucleoside transport, inhibits macromolecule synthesis, induces DNA fragmentation, and decreases the growth and viability of L1210 leukemic cells in the same nanomolar range as daunorubicin *in vitro*. Anticancer Drugs 11: 339-352, 2000.
16. Perchellet EM, Ward MM, Skaltsounis A-L, Kostakis IK, Pouli N, Marakos P and Perchellet J-P: Antiproliferative and proapoptotic activities of pyranoxanthenones, pyranothioxanthenones and their pyrazole-fused derivatives in HL-60 cells. Anticancer Res 26: 2791-2804, 2006.
17. Morgan AR, Lee JS, Pulleyblank DS, Murray NL and Evans DH: Ethidium fluorescence assays. Part 1. Physico-chemical studies. Nucleic Acids Res 7: 547-569, 1979.
18. Perchellet EM, Wang Y, Weber RL, Sperfslage BJ, Lou K, Crossland J, Hua DH and Perchellet J-P: Synthetic 1,4-anthracenedione analogs induce cytochrome *c* release, caspase-9, -3, and -8 activities, poly(ADP-ribose) polymerase-1 cleavage and internucleosomal DNA fragmentation in HL-60 cells by a mechanism which involves caspase-2 activation but not Fas signaling. Biochem Pharmacol 67: 523-537, 2004.
19. Fenech M, Chang WP, Kirsch-Volders M, Holland N, Bonassi S and Zeiger E: HUMN project: detailed description of the scoring criteria for the cytokinesis-block micronucleus assay using isolated human lymphocyte cultures. Mutat Res 534: 65-75, 2003.
20. Wang Y, Perchellet EM, Tamura M, Hua DH and Perchellet J-P: Induction of poly(ADP-ribose) polymerase-1 cleavage by antitumor triptycene bisquinones in wild-type and daunorubicin- resistant HL-60 cell lines. Cancer Lett 188: 73-83, 2002.
21. Ge J, Normant E, Porter JR, Ali JA, Dembski MS, Gao Y, Georges AT, Grenier L, Pak RH, Patterson J, Sydor JR, Tibbitts TT, Tong JK, Adams J and Palombella VJ: Design, synthesis and biological evaluation of hydroquinone derivatives of 17-amino-17-demethoxygeldanamycin as potent, water-soluble inhibitors of Hsp90. J Med Chem 49: 4606-4615, 2006.
22. Lieu C-H, Chang Y-N and Lai Y-K: Dual cytotoxic mechanisms of submicromolar taxol on human leukemia HL-60 cells. Biochem Pharmacol 53: 1587-1596, 1997.
23. Duriez PJ and Shah GM: Cleavage of poly(ADP-ribose) polymerase: a sensitive parameter to study cell death. Biochem Cell Biol 75: 337-349, 1997.
24. Scaltriti M and Baselga J: The epidermal growth factor receptor pathway: a model for targeted therapy. Clin Cancer Res 12: 5268-5272, 2006.
25. Isaacs JS, Xu W and Neckers L: Heat shock protein 90 as a molecular target for cancer therapeutics. Cancer Cell 3: 213-217, 2003.
26. Kamal A, Boehm MF and Burrows FJ: Therapeutic and diagnostic implications of Hsp90 activation. Trends Mol Med 10: 283-290, 2004.
27. Roe SM, Prodromou C, O'Brien R, Ladbury JE, Piper PW and Pearl LH: Structural basis for inhibition of the Hsp90 molecular chaperone by the antitumor antibiotics radicicol and geldanamycin. J Med Chem 42: 260-266, 1999.
28. Yarden Y and Sliwkowski MX: Untangling the ErbB signaling network. Nat Rev Mol Cell Biol 2: 127-137, 2001.

29. Rusnak DW, Affleck K, Cockerill SG, Stubberfield C, Harris R, Page M, Smith KJ, Guntrip SB, Carter MC, Shaw RJ, Jowett A, Stables J, Topley P, Wood ER, Brignola PS, Kadwell SH, Reep BR, Mullin RJ, Alligood KJ, Keith BR, Crosby RM, Murray DM, Knight WB, Gilmer TM and Lackey K: The characterization of novel, dual ErbB-2/EGFR, tyrosine kinase inhibitors: potential therapy for cancer. Cancer Res 61: 7196-7203, 2001.
30. Rabindran SK, Discafani CM, Rosfjord EC, Baxter M, Floyd MB, Golas J, Hallett WA, Johnson BD, Nilakantan R, Overbeek E, Reich MF, Shen R, Shi X, Tsou H-R, Wang Y-F and Wissner A: Antitumor activity of HKI-272, an orally active, irreversible inhibitor of the HER-2 tyrosine kinase. Cancer Res 64: 3958-3965, 2004.
31. Perchellet EM, Magill MJ, Huang X, Brantis CE, Hua DH and Perchellet JP: Triptycenes: a novel synthetic class of bifunctional anticancer drugs that inhibit nucleoside transport, induce DNA cleavage and decrease the viability of leukemic cells in the nanomolar range *in vitro*. Anticancer Drugs 10: 749-766, 1999.
32. Gewirtz DA: A critical evaluation of the mechanisms of action proposed for the antitumor effects of the anthracycline antibiotics adriamycin and daunorubicin. Biochem Pharmacol 57: 727-741, 1999.
33. Shi Q and King RW: Chromosome non-disjunction yields tetraploid rather than aneuploid cells in human cell lines. Nature 437: 1038-1042, 2005.
34. Nagata S: Apoptotic DNA fragmentation. Exp Cell Res 256: 12-18, 2000.
35. Herceg Z and Wang ZQ: Functions of poly(ADP-ribose) polymerase (PARP) in DNA repair, genomic integrity and cell death. Mutat Res 477: 97-110, 2001.
36. Perchellet EM, Wang Y, Weber RL, Lou K, Hua DH and Perchellet J-P: Antitumor triptycene bisquinones induce a caspase-independent release of mitochondrial cytochrome *c* and a caspase-2-mediated activation of initiator caspase-8 and -9 in HL-60 cells by a mechanism which does not involve Fas signaling. Anticancer Drugs 15: 929-946, 2004.
37. Li P, Nijhawan D, Budihardjo I, Srinivasula SM, Ahmad M, Alnemri ES and Wang X: Cytochrome *c* and dATP-dependent formation of Apaf-1/Caspase-9 complex initiates an apoptotic protease cascade. Cell 91: 479-489, 1997.
38. Wang Y, Perchellet EM, Ward MM, Lou K, Zhao H, Battina SK, Wiredu B, Hua DH and Perchellet JP: Antitumor triptycene analogs induce a rapid collapse of mitochondrial transmembrane potential in HL-60 cells and isolated mitochondria. Int J Oncol 28: 161-172, 2006.
39. Perchellet EM, Wang Y, Lou K, Zhao H, Battina SK, Hua DH and Perchellet JP: Antitumor triptycene analogs directly interact with isolated mitochondria to rapidly trigger markers of permeability transition. Anticancer Res 27: 3259-3272, 2007.
40. Walter L, Miyoshi H, Leverve X, Bernardi P and Fontaine E: Regulation of the mitochondrial permeability transition pore by ubiquinone analogs. A progress report. Free Radic Res 36: 405-412, 2002.
41. Alano CC, Ying W and Swanson RA: Poly(ADP-ribose) polymerase-1-mediated cell death in astrocytes requires NAD^+ depletion and mitochondrial permeability transition. J Biol Chem 279: 18895-18902, 2004.
42. Whitesell L and Lindquist SL: HSP90 and the chaperoning of cancer. Nat Rev Cancer 5: 761-772, 2005.
43. Zhang H and Burrows F: Targeting multiple signal transduction pathways through inhibition of Hsp90. J Mol Med 82: 488-499, 2004.